10-16-2020

# Quantum oscillations with angular dependence in PdTe2single crystals

Ramakanta Chapai
*Louisiana State University*

D. A. Browne
*Louisiana State University*

David E. Graf
*National High Magnetic Field Laboratory*

J. F. Ditusa
*Louisiana State University*

Rongying Jin
*Louisiana State University*



## Recommended Citation

Chapai, R., Browne, D., Graf, D., Ditusa, J., & Jin, R. (2020). Quantum oscillations with angular dependence in PdTe2single crystals. *Journal of Physics Condensed Matter, 33* (3) https://doi.org/10.1088/1361-648X/abb548

# Quantum Oscillations with Angular Dependence in $PdTe_2$ Single Crystals

Ramakanta Chapai[1], D. A. Browne[1], David E. Graf[2], J. F. DiTusa[1], and Rongying Jin[1,*]

[1]*Department of Physics and Astronomy, Louisiana State University, Baton Rouge, LA 70803*, USA

[2]*National High Magnetic Field Laboratory, Tallahassee, FL 32310*, USA

## Abstract

The layered transition-metal dichalcogenide $PdTe_2$ has been discovered to possess bulk Dirac points as well as topological surface states. By measuring the magnetization (up to 7 T) and magnetic torque (up to 35 T) in single crystalline $PdTe_2$, we observe distinct de Haas-van Alphen (dHvA) oscillations. Eight frequencies are identified with $H$ // $c$, with two low frequencies ($F_\alpha$ = 8 T and $F_\beta$ = 117 T) dominating the spectrum. The effective masses obtained by fitting the Lifshitz-Kosevich equation to the data are $m_\alpha^* = 0.059m_0$ and $m_\beta^* = 0.067m_0$ where $m_0$ is the free electron mass. The corresponding Landau fan diagrams allow the determination of the Berry phase for these oscillations resulting in values of ~ 0.67π for the 3D α band (hole-type) (down to the 1st Landau level) and ~ 0.23π - 0.73π for the 3D β band (electron-type) (down to the 3rd Landau level). By investigating the angular dependence of the dHvA oscillations, we find that the frequencies and the corresponding Berry phase ($\Phi_B$) vary with the field direction, with a $\Phi_B \sim 0$ when $H$ is 10° - 30° away from the *ab* plane for both α and β bands. The multiple band nature of $PdTe_2$ is further confirmed from Hall effect measurements.

Keywords: topological materials, de Haas-van Alphen oscillations, Landau levels, Berry phase

[*]*Corresponding author: rjin@lsu.edu*

## Introduction

Due to the versatility of crystal symmetry operations, condensed matter systems are fertile ground to realize new physics involving novel particle excitations such as Dirac fermions [1-3], Weyl fermions [4, 5], Majorana fermions [6, 7], and even more complex or exotic fermions [8, 9]. Realizing these excitations in solids not only offers opportunities to investigate the fundamental physics associated with these excitations, but also provides powerful routes towards potential applications such as quantum computing and spintronic technologies [10-12]. In this regard, materials with unique quantum mechanical properties such as topological insulation and topological superconductivity have attracted a great deal of recent attention [13, 14]. Among quantum materials, the layered transition metal dichalcogenides (TMDs) present a wide variety of intriguing properties. For example, the coexistence of type-I Dirac fermions and type-II Dirac fermions has been reported in some layered TMDs [15]. In type-I Dirac fermion systems, the valence and conduction bands meet at the Dirac point and Lorentz invariance is obeyed. In contrast, type-II Dirac fermions break Lorentz invariance because of the tilting of the Dirac cones [16]. Consequently, new quantum phenomena such as the angle dependent chiral anomaly and topological phase transitions are expected in the type-II Dirac fermion systems [16-20].

The presence of type-II Dirac fermions in $PdTe_2$ was recently predicted by first principles calculations and observed in angle-resolved photoemission spectroscopy (ARPES) [17, 21]. In addition to possessing topologically non-trivial bulk bands and topological surface states [15, 22], $PdTe_2$ exhibits superconductivity as well (with $T_c \sim 1.7$ K [21, 23]). Thus, it is likely a candidate for topological superconductivity [21]. However, there is considerable disparity in experimental results in literature. As summarized in Table I, we note that (1) some frequencies obtained from quantum oscillations are not consistent with each other [21, 24-28], (2) there is large discrepancy in the Berry phase for the smallest band [21, 24-26], and (3) there is little information about the larger bands other than the one with the lowest frequency. These conflicting results call for continued examination of the physical properties of $PdTe_2$. This is in part due to its complex Fermi surface and the associated difficulty in identifying the contribution of each Fermi surface pocket to the overall transport properties [21, 24, 25]. It has also not been addressed whether these discrepancies are related to sample quality (composition and crystallinity). Moreover, a measurement of the angle dependence of the Berry phase, which is crucial to understand the

Fermi surface topology, has not been reported.

Table I: A list of frequency $F$ (in the unit of Tesla) and Berry phase $\Phi_B$ (in the unit of $\pi$) that have been detected from de Haas-van Alphen (dHvA) and Shubnikov-de Haas (SdH) oscillations in $PdTe_2$ with $H$ // c.

| This work (dHvA) | | Ref. [21] (dHvA) | | Ref. [24] | | | Ref. [25] (dHvA) | Ref. [26] (dHvA) | | Ref. [27] (dHvA) | Ref. [28] (dHvA) |
|---|---|---|---|---|---|---|---|---|---|---|---|
| | | | | dHvA | | SdH | | | | | |
| $F$ | $\Phi_B$ | $F$ | $\Phi_B$ | $F$ | $\Phi_B$ | $F$ | $F$ | $F$ | $\Phi_B$ | $F$ | $F$ |
| 8 ($\alpha$) | 0.67 | 8.0 | 0.92 | 8 | 1.14 | - | - | 9.13 | 0.72 | 9 | - |
| - | - | - | - | 109 | - | - | - | - | - | - | - |
| - | - | 113.2 | - | 113 | - | - | - | 112.7 | - | 112 | - |
| 117 ($\beta$) | 0.23 | 117.9 | - | 117 | - | - | 121.5 | - | - | - | - |
| - | - | 124.3 | - | 127 | - | - | - | - | - | - | 125 |
| 133 ($\gamma$) | - | 133.9 | - | 133 | - | - | - | - | - | - | - |
| 141 ($\alpha+\gamma$) | - | - | - | 140 | - | - | - | - | - | - | - |
| 242 ($\alpha+2\beta$) | - | - | - | - | - | - | 239 | 228.7 | - | - | - |
| 272 ($\eta$) | - | - | - | | - | - | 283.2 | - | - | - | - |
| 360 ($\zeta$) | - | - | - | - | - | - | - | - | - | - | - |
| 462($\wp$) | - | 455.8 | - | 455 | - | - | - | 456.9 | - | 459 | 460 |
| - | - | - | - | - | - | 920 | - | 913.9 | - | - | - |
| 2468 ($\vartheta$) | - | - | - | - | - | 2350 | - | - | - | - | 2260 |
| 2588 ($\xi$) | - | - | - | - | - | 2675 | - | 2568 | - | 2577 | 2560 |

Here, we describe the results of an experimental investigation of the magnetotransport (magnetoresistance and Hall effect) and magnetic (magnetization and magnetic torque) properties of $PdTe_2$ to explore the nature of the electronic excitations. By analyzing the de Haas-van Alphen (dHvA) oscillations found in both the magnetization and magnetic torque at low temperatures, eight frequencies are identified: $F_\alpha$ = 8 T, $F_\beta$ = 117 T, $F_\gamma$ = 133 T, $F_\eta$ = 272 T, $F_\zeta$ = 360 T, $F_\wp$ = 462 T, $F_\vartheta$ = 2468 T, and $F_\xi$ = 2588 T. The presence of multiple Fermi surface pockets is further confirmed by the Hall resistivity, which varies nonlinearly with the applied magnetic field. Using the Lifshitz-Kosevich equation [29] to fit experimental data, the effective masses of the respective bands are found as: $m_\alpha^* = 0.059m_0$, $m_\beta^* = 0.067m_0$, $m_\gamma^* = 0.084m_0$, $m_\eta^* = 0.107m_0$, and $m_\zeta^* = 0.120m_0$ ($m_0$ is the free electron mass). Two of these frequencies ($F_\alpha$ and $F_\beta$) have large oscillation amplitudes, allowing a precise assignment of oscillations to the Landau levels (LLs). Under 33 Tesla, electrons reach the 1st LL in the $\alpha$ band, and the 3rd LL in the $\beta$ band. By fitting the data with the Lifshitz-Onsager quantization criterion [30], we obtain the Berry phase ~ 0.67$\pi$ for the 3D $\alpha$ band with a hole character, and ~ 0.23$\pi$ - 0.73$\pi$ for the 3D $\beta$ band with an electron character at H // *c*. Further analysis of the angle dependence of the dHvA oscillations indicates

that the oscillation frequencies and associated Berry phases vary significantly with respect to the direction of the applied magnetic field. Especially, the change from non-zero to zero Berry phase is observed when $H$ is 10° - 30° away from the $ab$ plane for both α and β bands.

## Experiment

Single crystals of $PdTe_2$ were grown via the self-flux method using excess tellurium (Te) as flux in a molar ratio of Pd : Te = 1 : 2.2. The starting material, Pd powder (99.95%, Alfa Aesar) and Te powder (99.99%, Alfa Aesar), was mixed together and placed into an alumina crucible, which was then sealed in a quartz tube under a vacuum of ~ 10 millitorr. The tube was heated to 780 ℃ at 96 ℃/h in a furnace, held at 780 ℃ for 48 hours. The temperature was lowered to 500 ℃ with a rate of 3.6 ℃/h. After staying at this temperature for 80 hours, it was allowed to cool slowly to room temperature. Single crystals with typical size ~ 4 × 2.5 × 0.5 $mm^3$ were obtained (shown in the lower panel of Fig. S1(a) in the Supplementary Material).

The structure of as-grown crystals was examined through powder (crushed single crystals) X-ray diffraction (XRD) measurements using a *PANalytical* Empyrean X-ray diffractometer (Cu $K_\alpha$ radiation; λ=1.54187 Å). All the diffraction peaks can be indexed under a $CdI_2$-type trigonal structure (space group $P\bar{3}m1$ with the lattice parameter $a = b$ = 4.022 Å and $c$ = 5.115 Å (see Fig. S1(b) in the Supplementary material). The crystal symmetry and lattice parameters are consistent with previous reports [28, 31]. Notably, each lattice parameter in Ref. [25] is ~2.5% larger than ours. In the absence of any explanation in Ref. [25], we consider that the variation of lattice parameters is related to sample stoichiometry. For example, the sample in Ref. [26] is slightly Pd rich, and its lattice parameter $a$ is closer to that in Ref. [25], but $c$ is close to ours. Through the energy dispersive spectroscopy (EDS), our crystals have Pd : Te ~ 0.97 : 2 (see Fig. S1(d) in the Supplementary material). The Electrical resistivity was measured using the standard four-probe technique in a Physical Properties Measurement System (PPMS-14T, *Quantum Design*). The magnetization measurements were carried out in a Superconducting Quantum Interference Device magnetometer (MPMS-7T, *Quantum Design*). Magnetic torque measurements were performed using the piezo-resistive torque magnetometer with a 35 T resistive magnet at the National High Magnetic Field Laboratory (NHMFL) in Tallahassee, Florida. The de Haas-van Alphen (dHvA) oscillations were observed in both the magnetization and magnetic torque at low temperatures ($T$

≤ 25 K) and high magnetic fields ($H \geq 1.5$ T). The angle dependence of the magnetoresistance was also measured up to 35 T at NHMFL using the standard four-probe technique.

## Results and discussion

Figure 1(a) displays the temperature dependence of the electrical resistivity of $PdTe_2$ along the *ab* plane ($\rho_{ab}$). Note that $\rho_{ab}$ decreases with decreasing temperature in the whole temperature range between 2 and 400 K with $\rho_{ab}$(300 K) ~ 36.8 μΩ cm and $\rho_{ab}$ (2 K) ~ 0.79 μΩ cm, yielding the residual resistivity ratio (RRR) of $\rho_{ab}$ (300 K)/$\rho_{ab}$ (2 K) ~ 47. Such a high RRR value and low residual resistivity reflect the high quality of our single crystals. At high temperatures (50 K - 400 K), $\rho_{ab}(T)$ is well described by the Bloch-Gruneisen (BG) formula [32]

$$\rho(T) = \rho(0) + B_{e-ph}(T/\theta_D)^5 \int_0^{T/\theta_D} dx x^5 / \{[(e^x - 1)(1 - e^{-x})]\}, \quad (1)$$

Here, $T$ is the temperature, $\rho(0)$ is the residual resistivity, $\theta_D$ is the Debye temperature and $B_{e\text{-}ph}$ is a constant representing the scattering strength of electrons with acoustic phonons. From the fit, we obtain $\theta_D$ ~ 245 K and $B_{e\text{-}ph}$ ~ 122 μΩ cm. The $\theta_D$ determined in this manner is slightly higher than that obtained from specific heat measurements [33]. At low temperatures, the experimental data gradually deviates from the BG formula. Below 30 K, the data can be fit to $\rho_{ab}(T) = \rho(0) + AT^m$ with $\rho(0)$ = 0.75 μΩ cm, and $m$ ~ 3 (see the inset of Fig. 1(a)). This indicates dominant inter-band electron-phonon scattering [34] at low temperatures (rather than intra-band electron-phonon or electron-electron scattering), which is consistent with a previous report [24]. Figure 1(b) shows the temperature dependence of the magnetic susceptibilities along the *ab*-plane ($\chi_{ab}$) and *c* axis ($\chi_c$) between 2 to 400 K measured in an applied magnetic field of 1 kOe. In the whole temperature range, $\chi_c$ is small but positive and slowly increases with decreasing temperature. Overall, both $\chi_{ab}$ and $\chi_c$ are rather small in magnitude. While $\chi_{ab}$ is negative and almost temperature independent in a wide temperature range, $\chi_c$ is positive and increases with decreasing temperature. The linear field dependence of the magnetization $M_{ab}$ (shown in Fig. S4(a) in the Supplementary material), indicates that the diamagnetism results from Pd and Te cores. On the other hand, the positive $\chi_c$ should be attributed to slight non-stoichiometry of the sample, which impacts more along the *c* direction. The positive $\chi_c$ was also observed in Ref. [24] but not in Ref. [21].

While $\chi_c$ is small, the electrical transport exhibits a large response to the application of a magnetic field, $H$. Figure 1(c) displays the transverse ($H$ // $c$, $I$ // $ab$) magnetoresistance $MR_{ab} = [\rho_{ab}(H) - \rho_{ab}(0)]/\rho_{ab}(0)$ measured at a variety of temperatures. $MR_{ab}$ is positive at all temperatures measured and increases with decreasing temperature. For a given temperature, $MR_{ab}$ increases with increasing field, showing no sign of saturation. At 2 K and $H$ = 14 T, it reaches 350%, close to values previously reported [25]. For a non-magnetic metallic system, such large and positive MR is unusual, and cannot be simply attributed to the curving of electron trajectories under the application of magnetic field [35, 36].

For a system with either a single band (or a dominant single band) or multiple bands with electron-hole compensation, the $MR$ is expected to follow the Kohler's law [37], i.e., all data collapses into a single curve when plotted $MR_{ab}$ versus $H/\rho_{ab}(0)$. Fig. 1(d) shows such a plot for $PdTe_2$, with all data scaling well. The scaling curve is well described by the form $MR_{ab} = 7.45(H/\rho_{ab}(0))^{1.3}$ as represented by the solid line in Fig. 1(d). This indicates a deviation from the expected standard Kohler form where $MR \propto H^2$. Similar behavior has been observed in other semimetals [38, 39]. The lower power (< 2) in the field dependence is attributed to a linear-$H$ component that is expected when approaching the quantum limit [24, 40]. In this sense, our $MR_{ab}$ would imply larger linear-$H$ component compared to that reported earlier for $PdTe_2$ where a $H^{1.9}$ dependence was found [24]. Nevertheless, the scaling behavior indicates that large $MR_{ab}$ is intrinsic and can be described by a single electron scattering rate. If the system contains magnetic impurities, electrons would experience more than one type of scattering, impossible to hold the scaling behavior.

To further understand the $H$ dependence of the magnetoresistance, we measured $MR_{ab}$ with different field direction as displayed in Fig. 1(e). Note that $MR_{ab}$ is always positive for all orientation from $H \perp I$ (transverse $MR_{ab}$) to $H$ // $I$ (longitudinal $MR_{ab}$) with a progressive decrease in magnitude as the longitudinal orientation is approached. In addition, there is an obvious curvature change from $\theta = 0°$ to 90°, similar to what was observed in Ref. [26]. This indicates the change of the $H$ dependence of $MR_{ab}$. In addition to the reduced contribution from the Lorentz force upon the increase of $\theta$, the curvature changes for $\theta > 60°$ may be related to a change in the band topology, as will be discussed later. By fitting the high-field $MR$ data (above 10 T) using $MR(H) \propto H^{\kappa}$, we determine the exponent $\kappa$ for each $\theta$, which is presented in the inset of Fig. 1(e). Note that there is a sharp decrease of $\kappa$ at $\theta > 60°$. Nevertheless, the longitudinal $MR_{ab}$ tends

to saturate at much smaller field as expected for a conventional semimetal, even though the amplitude of the magnetoresistance is still unusually high.

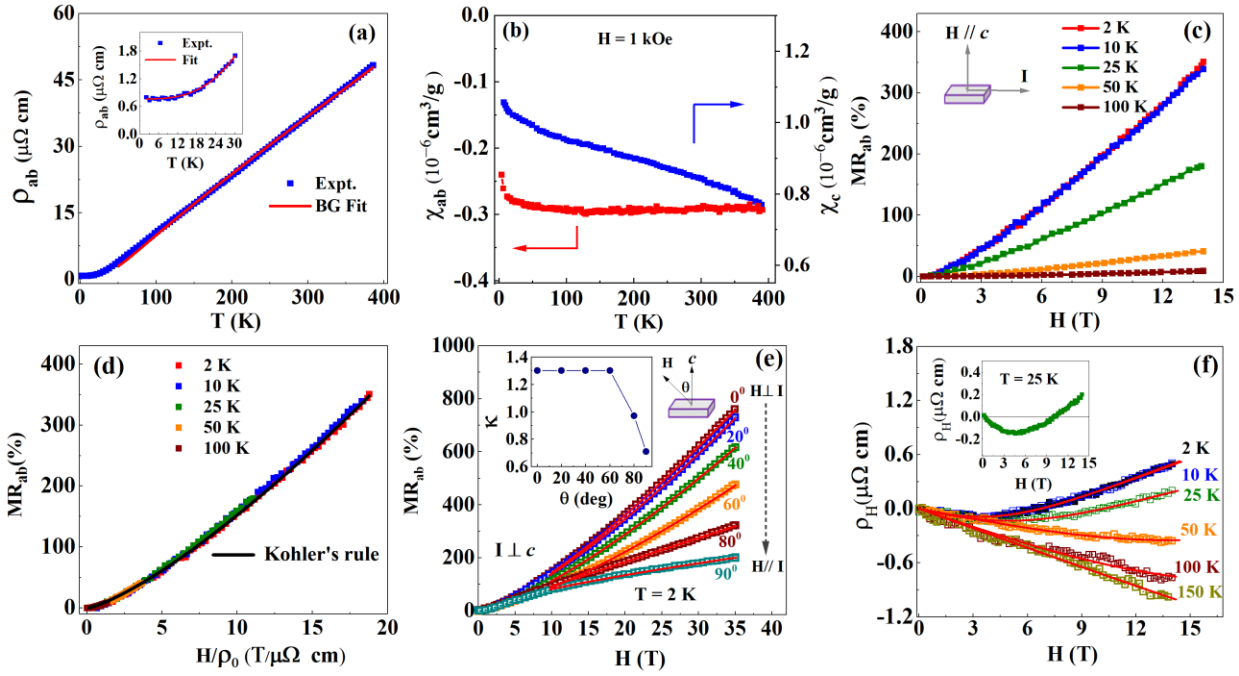


FIG. 1. (a) Temperature ($T$) dependence of the electrical resistivity ($\rho_{ab}$) of $PdTe_2$. Solid line is a fit of Eq. (1) to the data. Upper left inset: $\rho_{ab}$ versus $T$. Solid line is a fit of the form $\rho = \rho(0) + AT^m$ to the data. (b) $T$ dependence of the magnetic susceptibility along the $ab$ plane $\chi_{ab}$ (red) and the $c$ axis $\chi_c$ (blue) measured by applying a magnetic field, $H$=1 kOe. (c) Transverse magnetoresistance $MR_{ab}$ at indicated temperatures; (d) Kohler scaling plot produced using the data in frame (c). Solid line is a fit of the Kohler form to the data. (e) $MR_{ab}$ measured up to 35 T at 2 K for various angles between $H$ // $c$ and $H$ // $ab$ with the angle defined in the inset. Red lines represent fits of the data above 10 T to a power law $MR \propto H^{\kappa}$. Inset: angle dependence of the exponent $\kappa$. (f) Hall resistivity ($\rho_H$) measured at the temperatures indicated in the figure and the corresponding fits of Eq. (2) (red lines). Inset: Hall resistivity at 25 K displaying a sign change.

Figure 1(f) shows the field dependence of the Hall resistivity ($\rho_H$) at different temperatures. While $\rho_H$ varies linearly with $H$ with a negative slope at high temperatures, a nonlinearity in $\rho_H(H)$ (gradually develops and becomes obvious below 50 K, leading to a sign change at low temperatures and high $H$ (see the inset of Fig. 1(f)). The nonlinear Hall resistivity with a sign change clearly indicates a multiple band charge transport with contributions from both electron and hole Fermi surface pockets [21, 24, 28, 31]. Similar behavior was reported in Ref.

[21]. To further understand the nonmonotonic field dependence of the Hall resistivity, we use the two-band model [41, 42] to describe our experimental data,

$$\rho_{xy}(H) = \frac{H}{e}\frac{(n_h\mu_h^2 - n_e\mu_e^2) + (n_h - n_e)\mu_h^2\mu_e^2H^2}{(n_h\mu_h + n_e\mu_e)^2 + (n_h - n_e)^2\mu_h^2\mu_e^2H^2} \quad (2)$$

where $n_h(n_e)$ is the concentration of holes (electrons) and $\mu_h(\mu_e)$ is the mobility of holes (electrons). The fitting results are displayed in Fig. S2 (Supplementary material). While they show weak temperature dependence at high temperatures (> 50 K), both $n_h$ and $n_e$ decrease with decreasing temperature. At 2 K, $n_h \sim 1.6\times10^{22}$ cm$^{-3}$ and $n_e \sim 0.62\times10^{22}$ cm$^{-3}$, while $\mu_h \sim 0.11\times10^4$ cm$^3$ V$^{-1}$s$^{-1}$ and $\mu_e \sim 0.59\times10^4$ cm$^3$ V$^{-1}$s$^{-1}$. These mobilities are close to that of $PtTe_2$ [24] and $PtBi_2$ [39]. The carrier concentrations are close to that obtained from the thermopower measurement [43]. We also note that the ratio $n_h / n_e \neq 1$, implying uncompensated electrons and holes in $PdTe_2$.

Figure 2(a) displays the *H* dependence of the magnetization, *M*(*H*), measured along the *c* axis (*H* // *c*) at 1.8 K. Note that there are pronounced dHvA oscillations above 1.5 T. The emergence of the dHvA oscillations is the consequence of the Landau level formation in the presence of magnetic field [30, 44]. When the magnetic field varies, the quantized Landau levels pass over the Fermi surface, resulting in the oscillation of the electronic density of states (DOS) at the Fermi level. This leads to the oscillations of physical quantities including the magnetization and magnetic torque [13]. In the low field regime, a non-linear behavior can be seen for each temperature measured (see the inset of Fig. 2(a)). As discussed above, the non-linear *M*(*H*) is likely associated with the slight non-stoichiometry of the sample. However, whether the background is positive (Ref. [24]) or negative (Ref. [21]) does not seem to impact the dHvA oscillations, judged from observed frequencies (see Table I). The non-oscillatory part (smooth background) of the magnetization data is obtained by fitting the low-field magnetization using polynomial formula (the orange curve), which is subtracted from the data to obtain the oscillatory part of the magnetization Δ*M*, as plotted in Fig. 2(b). From the Fast Fourier Transformation (FFT) of these data shown in Fig. 2(c), two oscillations are identified with the frequencies $F_\alpha$ = 8 T and $F_\beta$ = 117 T.

According to the Lifshitz-Kosevich (LK) formula [29, 44],

$$\Delta M \propto -H^{1/2} \frac{A(\frac{m^*}{m_0})T}{\sinh(A(\frac{m^*}{m_0})T)} \exp\{-A(\frac{m^*}{m_0})T_D\} \cos(\pi g m^* / 2m_0) \sin[2\pi\{\frac{F}{H} - (\frac{1}{2} - \Phi)\}], \quad (3)$$

where $\frac{A(\frac{m^*}{m_0})T}{\sinh(A(\frac{m^*}{m_0})T)}$ is the thermal damping factor, $\exp\{-A(\frac{m^*}{m_0})T_D\}$ is the Dingle damping factor, $T_D$ is the Dingle temperature, $\cos(\pi g m^* / 2m_0)$ is the spin reduction factor, $A = \frac{2\pi^2 k_B m_0}{e\hbar H}$, $m^*$ is the effective mass of electron; and $g$ is the Landé factor. In addition, $\Phi = \frac{\Phi_B}{2\pi} + \delta$ where $\Phi_B$ is the Berry phase and δ = 0 for a two-dimensional (2D) and +/- 1/8 for a three-dimensional (3D) Fermi surface (FS), where +/- sign corresponds to the minima (+)/maxima (-) of the cross-sectional area of the FS for the case of an electron band. For a 3D hole band, the sign of δ is opposite [45]. The phase analysis of these dHvA oscillations makes it possible to reveal the topological properties of the associated carriers through the determination of $\Phi_B$. A non-zero value of $\Phi_B$ corresponding to the dHvA oscillation is an indication of the presence of non-trivial topology [44].

Fig. 2(d) exhibits the temperature dependence of the FFT amplitudes for both the α and β bands. From a fit of the thermal damping factor $\frac{A(\frac{m^*}{m_0})T}{\sinh(A(\frac{m^*}{m_0})T)}$ to the temperature dependence of the FFT amplitude, we obtain $m_\alpha^* = 0.060 m_0$ and $m_\beta^* = 0.068 m_0$. Both of these values are smaller than that reported previously [21] but somewhat larger than that reported in Ref. [24].

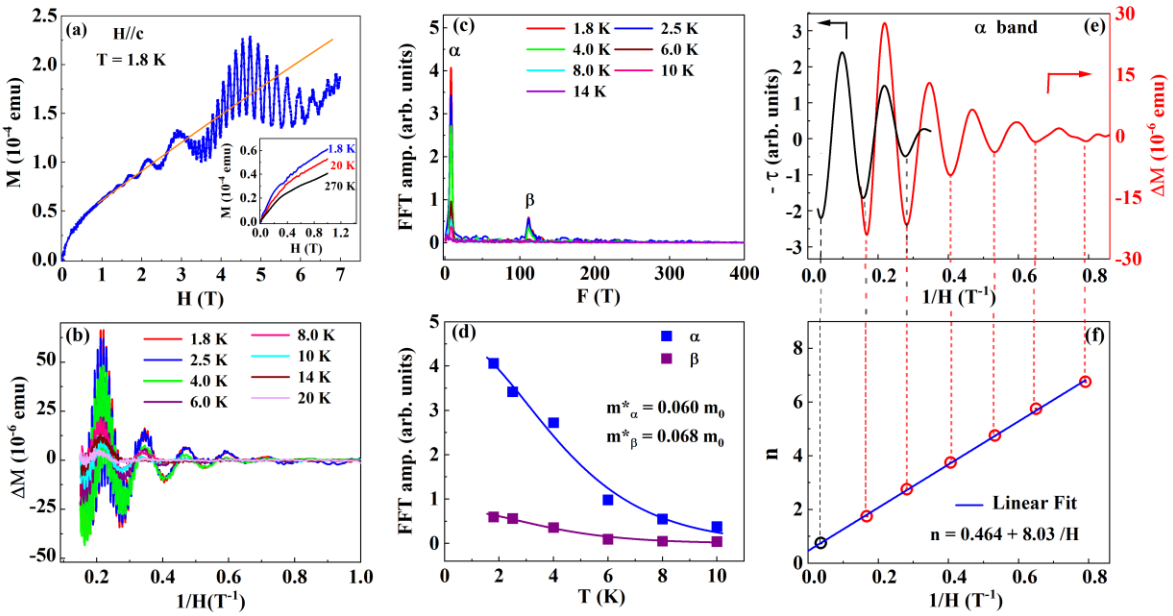


FIG. 2. (a) Magnetization ($M$), vs. magnetic field ($H$) of $PdTe_2$ at 1.8 K; Inset: Low-field $M(H)$ at the indicated temperatures. Orange line represents the non-oscillatory part (smooth background) of the magnetization. (b) dHvA oscillations after the subtraction of the non-oscillatory part of $M$ ($\Delta M$) at the indicated temperatures; (c) FFT of $\Delta M$ at the indicated temperatures. (d) Temperature dependence of the FFT amplitude observed in frame (c) for the α and β bands. Solid lines are fits with thermal damping term of Eq. (3); (e) dHvA oscillation of $\Delta M$ (red) and τ (black) at 1.8 K. (f) Landau fan diagram constructed from the dHvA oscillation corresponding to the α band in $\Delta M$ in frame (e).

According to the Onsager relation, $F = (\Phi_0/2\pi^2)S$, where $\Phi_0$ is the flux quanta and $S$ is the cross-section area of the Fermi surface normal to the $H$ direction. For the α band, we found $S_\alpha \sim 0.076$ nm$^{-2}$, which corresponds to the Fermi wave vector $k_\alpha \sim 0.015$ Å$^{-1}$. This wave vector is close to that of expected from DFT calculations for a small hole pocket around the Γ point [21, 24] of the Brillouin Zone (BZ). We notice that the dHvA oscillation due to the α band was not detected in Ref. [25], suggesting that the Fermi level is sample sensitive as suggested in Ref. [24]. For the β band, we find $S_\beta \sim 1.115$ nm$^{-2}$ and the corresponding Fermi wave vector $k_\beta \sim 0.059$ Å$^{-1}$. This value is close to that corresponding to the electron pocket located between A to H points in the BZ as reported in the published DFT calculations [15, 21].

To assign Landau levels for each oscillation, we separate ΔM for each frequency via the filtering process [24, 45]. Figure 2(e) shows $\Delta M$ versus $1/H$ (red curve) for the α band isolated by using a low-pass filter of 20 T. The Landau fan diagram can be constructed by assigning the oscillation minima to $n$-1/4 with $n$ being the Landau level index [44]. As shown in Fig. 2(f), $n(H$

[1]) can be fitted with the Lifshitz-Onsager quantization criterion [30] as $n$ = 0.46 + 8.03/H. From the fit, we obtain the frequency $F_\alpha$ = 8.03 T, in excellent agreement with that obtained from the FFT spectra. This implies that the filtering process to isolate the α band preserves the original signal. The intercept of this linear equation gives the Berry phase as $(\Phi_B^\alpha / 2\pi) + \delta = 0.46$, i.e. $\Phi_B^\alpha = 0.92\pi - 2\pi\delta$. Similar intercept value was also reported in Refs. [21, 24]. However, the corresponding Berry phase is considered to be nontrivial in Ref. [21] but trivial in Ref. [24] due to different interpretations of calculated electronic structures. In either case, the dimensionality factor (δ) has been completely ignored [21, 24, 26, 27]. According to Ref. [21], the α band corresponds to a hole pocket and nearly isotropic (to be discussed later), δ = 1/8 is expected corresponding to the maximum cross-section [46] for $H$ // $c$. We thus obtain the Berry phase $\Phi_B^\alpha = 0.67\pi$, indicating a topologically nontrivial phase. The nontrivial topology of the α band is consistent with the theoretical calculations (tilted Dirac cone along the Γ – A direction hosting type-II Dirac fermions) and ARPES measurements [17, 21].

Under 7 T, the carriers in the α band can reach the 2nd Landau level (LL), while the carriers in the β band are far from the quantum limit. The intercept obtained from the linear extrapolation from such high LLs will have a large uncertainty. To better determine the high field intercept and hence the precise Berry phase, we have carried out magnetic torque measurements of $PdTe_2$ for fields up to 35 T. Figure 3(a) shows the field dependence of the magnetic torque measured under $H$ // $c$ at several temperatures. As expected, the dHvA oscillations become more pronounced upon an increase of $H$. The dHvA oscillations plotted against the inverse magnetic field ($H^{-1}$) are shown in Fig. 3(b). Through the FFT analysis as shown in Fig. 3(c), we can identify eight frequencies, which are α (8 T), β (117 T), γ (133 T), η (272 T), ζ (360 T), ℘ (462 T), ϑ (24 68 T), and ξ (2588 T). While six of these frequencies (8 T, 117 T, 133 T, 462 T, 2468 T, and 2588 T) have been reported previously [21, 24], both η (272 T) and ζ (360 T) are new findings. Two additional peaks in Fig. 3(c) correspond to the sum of α and γ of 141 T and the sum of α and 2β of 242 T. Two high frequencies (2468 T and 2588 T) we observed were reported in Ref. [24] but not in Refs. [21,25]. As summarized in Table S1 (Supplementary material), literature shows discrepancies in the frequencies, which may be related to the subtle difference between samples or the method employed to measure them. This suggests that the Fermi surface pockets in $PdTe_2$ have not been well characterized [28].

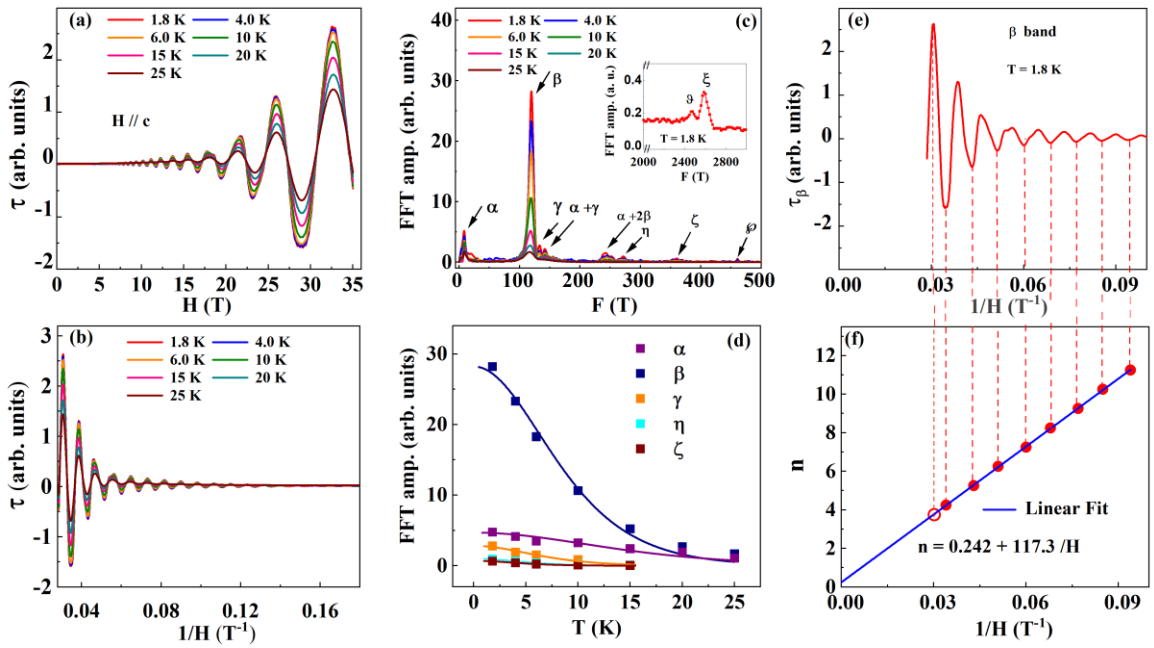


FIG.3. (a) Field dependence of the magnetic torque (τ) of $PdTe_2$ at the indicated temperatures; (b) τ versus 1/*H*. (c) FFT of τ at the indicated temperatures, Inset: FFT of τ at 1.8 K displaying high frequencies. (d) Variation of FFT amplitude with temperature for respective bands as indicated. The solid lines are fits with thermal damping term of Eq. (3). (e) dHvA oscillation at 1.8 K from the β band. (f) Landau fan diagram constructed from the data presented in frame (e).

Figure 3(d) displays the temperature dependence of the FFT amplitude for each of the frequencies identified. The FFT amplitude decreases with increasing temperature for all frequencies as expected. Fitting our data using the thermal damping term of Eq. (3), we obtain the effective mass of the carriers for each band. These results are summarized in Table II along with $S_F$ and $k_F$. Note that $m^*_\alpha$ and $m^*_\beta$ extracted from the magnetic torque are almost identical to those obtained from $M(H)$. The high $m^*_\eta$ compared to $m^*_\gamma$ suggests that $F_\eta$ is not the 2nd harmonic oscillation of the γ band. To investigate the dynamics of the carriers, we estimate $T_D$ through the Dingle plots (shown in Fig. S3, Supplementary material). From $T_D$, $m^*$ and $k_F$, we calculate the quantum relaxation time $\tau_q = \frac{\hbar}{2\pi T_D k_B}$, quantum mobility $\mu_q = \frac{e\tau_q}{m^*}$, Fermi velocity $v_F$, and mean free path $\lambda = v_F\tau_q$, which are listed in Table II. For the α band, the long $\tau_q$ and small $m^*$ lead to an extremely high quantum mobility, which is almost two times higher than that reported previously [21], reflecting high quality of our single crystal samples. Compared to the α band, the β band has much smaller $\tau_q$ and λ, even though its velocity is higher.

Table II: Parameters obtained from the dHvA oscillations in $PdTe_2$ at $H$ // $c$ including the oscillation frequency ($F$), the Fermi wave vector ($k_F$), the effective mass ($m^*$), the Fermi velocity ($v_F$), the Dingle temperature $T_D$, the quantum relaxation time ($\tau_q$) the quantum mobility ($\mu_q$)and the mean free path ($\lambda$).

| Band | $F$(T) | $S_F(10^{-2}$ Å$^{-2})$ | $k_F$(Å$^{-1}$) | $m^*/m_0$ | $v_F(10^5$ m/s) | $T_D$ (K) | $\tau_q(10^{-13}$ s) | $\mu_q$(m$^2$V$^{-1}$s$^{-1}$) | $\lambda$ (nm) |
|---|---|---|---|---|---|---|---|---|---|
| $\alpha$ | 8.0 | 0.076 | 0.015 | 0.059 | 2.9 | 2.30 | 5.0 | 1.465 | 145 |
| $\beta$ | 117 | 1.115 | 0.059 | 0.067 | 10.1 | 32.0 | 0.37 | 0.097 | 37.4 |
| $\gamma$ | 133 | 1.268 | 0.063 | 0.084 | 8.7 | _ | _ | _ | _ |
| $\eta$ | 272 | 2.593 | 0.090 | 0.107 | 9.7 | _ | _ | _ | _ |
| $\zeta$ | 360 | 3.432 | 0.104 | 0.120 | 9.9 | _ | _ | _ | _ |
| $\wp$ | 462 | 4.405 | 0.118 | _ | _ | _ | _ | _ | _ |
| $\vartheta$ | 2468 | 23.53 | 0.273 | _ | _ | _ | _ | _ | _ |
| $\xi$ | 2588 | 24.67 | 0.280 | _ | _ | _ | _ | _ | _ |

Since $\vec{\tau} = \vec{M} \times \vec{H}$ , the dHvA oscillations in the magnetic torque can be in phase or out of phase with that in the magnetization ( $\tau = -\frac{1}{F}\frac{dF}{d\theta} M_{//} H$ , where $M_{//}$ is the component of $M$ parallel to $H$ [44]). As shown in Fig. 2(e), $\tau$ (black) is out of phase with $\Delta M$. Nevertheless, dHvA oscillations obtained from $\tau$ overlaps well with that from $\Delta M$. Under 35 T, carriers in the $\alpha$ band reaches the 1st LL (Fig. 2(e)). By indexing the LLs from the dHvA oscillations corresponding to the $\beta$ band shown in Fig. 3(e), we find that high field (35 T) can push the carriers down to the 3rd LL. The oscillation due to the $\beta$ band is isolated via a band-pass filter centered about $F_\beta$, so to avoid possible contributions of other nearby frequencies. Although $F_\beta$ = 117 T has been reported [21, 24, 25], its Berry phase remains unknown. Figure 3(f) shows the Landau fan diagram for the $\beta$ band. From the intercept of the linear fit, we obtain $\Phi_B^\beta / 2\pi = 0.242 - \delta$. As the $\beta$ band is an electron pocket [21, 24], we find the Berry phase $\Phi_B^\beta = 0.23\pi$ (with $\delta$ = +1/8 for a FS minimum) - $0.73\pi$ (with $\delta$ = -1/8 for a maximum FS). While a non-zero $\Phi_B^\beta$ implies a nontrivial Berry phase, the $\beta$ band is not predicted to be involved in a nontrivial band crossing according to the DFT calculations in Ref. [21].

The angular dependence of quantum oscillations can provide further information about the Fermi surface topology. Figure 4(a) shows the magnetic torque at T = 4 K after background

subtraction plotted as $\Delta\tau$ ($H$) versus $H^{-1}$ for different angles θ as defined in the inset of Fig. 4(b). Upon the variation of θ, the dHvA oscillations change in both amplitude and peak position. Through the FFT analysis (see Fig. S5, Supplementary material), we can track the dominant α and β bands for all measured angles. However, the amplitudes associated with higher frequencies (γ, η, ζ, ℘, ϑ and ξ) gradually vanish at θ > 28°. To precisely analyze the amplitude variation with θ for the α and β bands, we separate their contributions through the band-pass filtering (shown in Fig. S6 and Fig. S7, Supplementary material). Figure 4(b) displays the angle dependence of the FFT amplitude for the α and β bands. The amplitude varies non-monotonically with θ for the both bands. Such non-monotonic variation of the FFT amplitude is attributed to the spin reduction factor $\cos(\pi g m^*/2m_0)$ (see Eq. (3)). Our measurement of the dHvA oscillations under $H$ // $ab$ (see Fig. S4 (d), Supplementary material) allows to determine $m^*_\alpha = 0.079m_0$ and $m^*_\beta = 0.092m_0$. These values of the effective masses are close to that found for $H$ // $c$. We therefore consider that the change in $m$* does not significantly alter $\cos(\pi g m^*/2m_0)$ and that the amplitude variation of the dHvA oscillations is due to the variation of $g$, which is related to spin-orbit coupling. When changing the magnetic field direction, a modification on the $g$ factor is expected [47]. When $g\frac{m^*}{m_0} = 2l+1$ ($l$ is an integer), the oscillation vanishes, a phenomenon known as the spin zero effect [44, 48]. Such an effect has been suggested for the band with 109 T frequency of $PdTe_2$ [24]. In contrast, our FFT amplitude data for both the α and β bands tends to vary greatly and is significantly reduced around 77° but does not completely vanish suggesting that the spin zero effect is not satisfied by these bands.

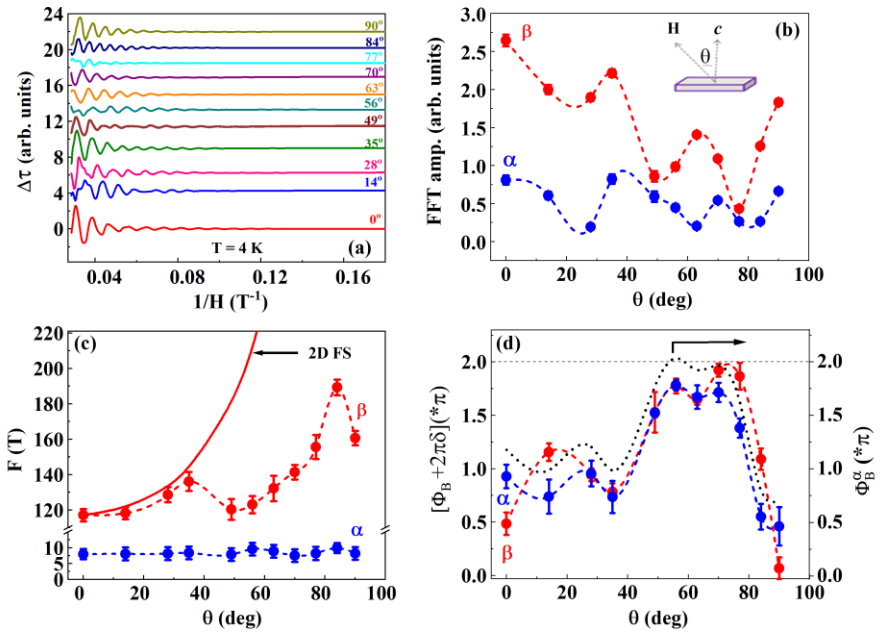

FIG. 4. (a) Magnetic torque of $PdTe_2$ at 4 K after background subtraction plotted as $\Delta\tau$ ($H$) versus $H^{-1}$ for different angles as indicated. A constant offset is added to the data for display purpose. (b) Angle dependence of the FFT amplitude for the α and β bands. (c) Angle dependence of $F_\alpha$ and $F_\beta$. The error bars are taken as the half-width at the half-height of the FFT peaks. Solid line represents the angular dependence expected for a 2D Fermi surface. (d) Angle dependence of $\Phi_B + 2\pi\delta$ for the α and β bands. Dotted line depicts the angle dependence of $\Phi_B$ for the α band assuming δ = 1/8. Dashed lines in (b-d) panels are guides to the eye.

Figure 4(c) displays the angle dependence of $F_\alpha$ and $F_\beta$. $F_\beta$ exhibits a non-monotonic angle dependence, while $F_\alpha$ is only weakly angle dependent. Apparently, neither the α nor β band possesses 2D Fermi surface character as represented by the solid curve in Fig. 4(c). While the angular dependence of $F_\alpha$ and $F_\beta$ has been previously reported up to θ ~60° [24], our data provides information in the range of $0^o \leq \theta \leq 90^o$. By constructing the Landau fan diagram from the dHvA oscillations at each angle measured (shown in Fig. S6 and Fig. S7, Supplementary material), the corresponding phase $\Phi_B + 2\pi\delta$ is extracted. Figure 4(d) displays $\Phi_B + 2\pi\delta$ versus angle for both α and β bands, both displaying a non-monotonic variation from $H$ // $c$ towards $H$ // $ab$. Despite the small anisotropy of the α frequency, $\Phi_B + 2\pi\delta$ strongly depends on the orientation of the applied field. If we assume δ = 1/8 for all field direction, $\Phi_B \sim 2\pi$ for the α band at 50° - 75°. As discussed earlier, there is a sharp change in the curvature of *MR* (see Fig. 1(e)) around 77°. Interestingly, the quantity $\Phi_B + 2\pi\delta$ for the β frequency also reaches 2π (i.e., zero) at 77° at which the oscillation amplitudes reach minimum. Understanding of the variation of the Berry phase with angle that we observe here requires further theoretical investigation.

## Summary

In summary, we have measured the charge transport properties (resistivity, magnetoresistance, and Hall resistivity), as well as the magnetic (magnetization and magnetic torque) properties of $PdTe_2$ single crystals with RRR ~ 47. While our magnetoresistance data exhibits Kohler-type scaling behavior, the MR displays an unusual $H^{1.3}$ dependence, suggesting contributions from multiple bands, as reflected in the Hall resistivity (with nonlinear-$H$ dependence and sign change). Pronounced dHvA oscillations are observed in the magnetization and magnetic torque at low temperatures. Through the analysis of the observed dHvA oscillations, eight bands are identified

with frequencies: 8 T, 117 T, 133 T, 272 T, 360 T, 462 T, 2468 T, and 2588 T for $H$ // $c$, the two intermediate frequencies (i.e. 272 T and 360 T) have not been previously reported, to our knowledge. Among these, the α band (8 T when $H$ // $c$) and β (117 T when $H$ // $c$) are the most dominant contributions. The angle dependence of $F_\alpha$ and $F_\beta$ indicates a 3D character of the corresponding bands. For the first time, the angle dependence of the Berry phase of the α and β bands of $PdTe_2$ are obtained, displaying a variation from nontrivial to trivial at an angle of 77° between $H$ and the crystallographic $c$ axis for the α and β bands. At present, it is not clear whether both the α and β bands are associated with a type-II Dirac cone which has been predicted to lie about 0.5 eV below the Fermi energy [21, 24].

**Acknowledgements**

This material is based upon work supported by the US Department of Energy under EPSCoR grant DE-SC0012432 with additional support from the Louisiana Board of Regents. A portion of this work was performed at the National High Magnetic Field Laboratory, which is supported by National Science Foundation Cooperative Agreement No. DMR-1644779 and the State of Florida.

**References**

[1] Borisenko S, Gibson Q, Evtushinsky D, Zabolotnyy V, Buchner B and Cava R J 2014 P*hys. Rev. Lett.* **113** 027603

[2] Neupane M, Xu S Y, Sankar R, Alidoust N, Bian G, Liu C, Belopolski I, Chang T R, Jeng H T, Lin H, Bansil A, Chou F and Hasan M Z 2014 *Nat. Commun.* **5** 3786

[3] Xu S Y, Liu C, Kushwaha S K, Sankar R, Krizan J W, Belopolski I, Neupane M, Bian G, Alidoust N, Chang T R *et al* 2015 *Science* **347** 294

[4] Weng H, Fang C, Fang Z, Bernevig B A and Dai X 2015 *Phys. Rev*. X **5** 011029

[5] Huang S, Kim J, Shelton W A, Plummer E W and Jin R 2017 *Proc. Natl. Acad. Sci.* **114** 6256

[6] Banerjee A, Bridges C A, Yan J Q, Aczel A A, Li L, Stone M B, Granroth G E, Lumsden M D, Yiu Y, Knolle J *et al* 2016 *Nat. Mater*. **15** 733

[7] He Q L, Pan L, Stern A L, Burks E C, Che X, Yin G, Wang J, Lian B, Zhou Q, Choi E S *et al* 2017 *Science* **357** 294

[8] Bradlyn B, Cano J, Wang Z, Vergniory M G, Felser C, Cava R J and Bernevig B A 2016 *Science* **353** 5037

[9] Chapai R, Jia Y, Shelton W A, Nepal R, Saghayezhian M, DiTusa J F, Plummer E W, Jin C and Jin R 2019 *Phys. Rev.* B **99** 161110(R)

[10] Chen Y L, Analytis J G, Chu J H, Liu Z K, Mo S K, Qi X L, Zhang H J, Lu D H, Dai X, Fang Z, Zhang S C, Fisher I R, Hussain Z and Shen Z X 2009 *Science* **325** 178

[11] Hasan M Z and Kane C L 2010 *Rev. Mod. Phys*. **82** 3045

[12] Hor Y S, Williams A J, Checkelsky J G, Roushan P, Seo J, Xu Q, Zandbergen H W, Yazdani A, Ong N P and Cava R J 2010 *Phys. Rev. Lett.* **104** 057001

[13] Ando Y J 2013 *Phys. Soc. Jpn*. **82** 102001

[14] Sato M and Ando Y 2017 *Rep. Prog. Phys*. **80** 076501

[15] Bahramy M S, Clark O J, Yang B J, Feng J, Bawden L, Riley J M, Markovic I, Mazzola F, Sunko V, Biswas D *et al* 2018 *Nat. Mater.* **17** 21

[16] Yan M, Huang H, Zhang K, Wang E, Yao W, Deng K, Wan G, Zhang H, Arita M, Yang H *et al* 2017 *Nat. Commun.* **8** 257

[17] Noh H J, Jeong J, Cho E J, Kim K, Min B I and Park B G 2017 *Phys. Rev. Lett*. **119** 016401

[18] Leng H, Paulsen C, Huang Y K and de Visser A 2017 *Phys. Rev.* B **96** 220506 (R)

[19] Yan B and Felser C 2017 *Annu. Rev. Condens. Matter Phys.* **8** 337

[20] Armitage N P, Mele E J and Vishwanath A 2018 *Rev. Mod. Phys.* **90** 015001

[21] Fei F, Bo X, Wang R, Wu B, Jiang J, Fu D, Gao M, Zheng H, Chen Y, Wang X *et al* 2017 *Phys. Rev.* B **96** 041201 (R)

[22] Liu Y, Zhao J Z, Yu L, Lin C T, Liang A J, Hu C, Ding Y, Xu Y, He S L and Zhao L *et al* 2015 *Chin. Phys. Lett.* **32** 067303

[23] Guggenheim J, Hulliger F and Muller J 1961 *Helv. Phys. Acta* **34** 408

[24] Zheng W, Schonemann R, Aryal N, Zhou Q, Rhodes D, Chiu Y C, Chen K W, Kampert E, Forster T, Martin T J, McCandless G T, Chan J Y, Manousakis E and Balicas L 2018 *Phys. Rev*. B **97** 235154

[25] Wang Y, Zhang J, Zhu W, Zou Y, Xi C, Ma L, Han T, Yang J, Wang J, Xu J *et al* 2016 *Sci. Rep.* **6** 31554

[26] Amit, Singh R K, Singh A, Wadehra N, Chakraverty S, Singh Y 2018 *Phys. Rev. Mater*. **2** 114202

[27] Das S, Amit, Sirohi A, Yadav L, Gayen S, Singh Y and Sheet G 2018 *Phys. Rev*. B **97** 014523

[28] Dunsworth A E 1975 *J. Low Temp. Phys*. **19** 51

[29] Lifshitz I E and Kosevich A M 1956 *Sov. Phys. JETP* **2** 636

[30] Ashcroft N W and Mermin N D 1976 *Solid State Physics* (New York: Holt, Rinehart and Winston)

[31] Jan J P and Skriver H L 1977 *J. Phys. F: Metal Phys*. **7** 1719

[32] Blatt F J 1968 *Physics of electronic conduction in solids* (New York: McGraw-Hill)

[33] Kudo K, Ishii H and Nohara M 2016 *Phys. Rev*. B **93** 140505(R)

[34] Ziman J M 2001 *Electrons and Phonons: The Theory of Transport Phenomena in Solids* (Oxford: Oxford University Press)

[35] Abrikosov A A 1988 *Fundamentals of the Theory of Metals* (Oxford: North-Holland)

[36] Pippard A B 1989 *Magnetoresistance in Metals* (Cambridge: Cambridge University Press)

[37] Duan F and Guojun J 2005 *Introduction to Condensed Matter Physics* Vol.1 (Singapore: World Scientific)

[38] Wang Y L, Thoutam L R, Xiao Z L, Hu J, Das S, Mao Z Q, Wei J, Divan R, Luican-Mayer A, Crabtree G W and Kwok W K 2015 *Phys. Rev*. B **92** 180402 (R)

[39] Xing L, Chapai R, Nepal R and Jin R 2020 *npj Quantum Mater.* **5** 10

[40] Wang K, Graf D and Petrovic C 2013 *Phys. Rev*. B **87** 235101

[41] Gao W, Hao N, Zheng F W, Ning W, Wu M, Zhu X, Zheng G, Zhang J, Lu J, Zhang H, Xi C, Yang J, Du H, Zhang P, Zhang Y, and Tian M 2017 *Phys. Rev. Lett.* **118** 256601

[42] Luo Y, Li H, Dai Y M, Miao H, Shi Y G, Ding H, Taylor A J, Yarotski D A, Prasankumar R P, and Thompson J D 2015 *Appl. Phys. Lett*. **107** 182411

[43] Hooda M K and Yadav C S 2018 *Europhys. Lett.* **121** 17001

[44] Shoenberg D 2009 *Magnetic Oscillations in Metals* (Cambridge: Cambridge University Press)

[45] Xia W, Shi X, Wang Y, Ge W, Su H, Wang Q, Wang X, Yu N, Zou Z, Hao Y, Zhao W, and Guo Y 2020 *Appl. Phys. Lett*. **116** 142103

[46] Li C, Wang C M, Wan B, Wan X, Lu H Z, Xie X C 2018 *Phys. Rev. Lett.* **120** 146602

[47] Gharaati A 2017 *Solid State Commun.* **258,** 17

[48] Bi R, Feng Z, Li X, Niu J, Wang J, Shi Y, Yu D and Wu X 2018 *New J. Phys.* **20** 063026